Dalton Transactions

Accepted Manuscript

ROYAL SOCIETY OF CHEMISTRY

www.rsc.org/dalton

Dalton Transactions

RSCPublishing

ARTICLE

Structure and Thermal Expansion in Tungsten Bronze $Pb_2KNb_5O_{15}$

Cite this: DOI: 10.1039/x0xx00000x

Kun Lin,[a] Hui Wu,[b,c] Fangfang Wang,[a] Yangchun Rong,[a] Jun Chen,[a] Jinxia Deng,[a,d] Ranbo Yu,[a] Liang Fang,[e] Qingzhen Huang,[b] and Xianran Xing*[,a]

Received 00th January 2012,
Accepted 00th January 2012

DOI: 10.1039/x0xx00000x

www.rsc.org/

Structure and thermal expansion behavior of tetragonal tungsten bronze oxide $Pb_2KNb_5O_{15}$ were investigated by neutron powder diffraction and high-temperature X-ray diffraction. Below Curie temperature T_C (orthorhombic phase, $T_C \approx 460$ °C), cell parameters a and c increase with temperature, while b decreases. The thermal expansion coefficients are $\alpha_a = 1.29\times10^{-5}$ °C^{-1}, $\alpha_b = -1.56\times10^{-5}$ °C^{-1}, and $\alpha_c = 1.62\times10^{-5}$ °C^{-1}. Temperature dependent of second harmonic generation (SHG), dielectric, and polarization-electrical field (P-E) hysteresis loops measurements were performed to study the symmetry and electric properties. We show that the distortion and cooperative rotation of NbO_6 octahedrons are directly responsible for negative thermal expansion coefficient along polar b axis. It is suggested that Pb-O covalency, especially in the large and asymmetry pentagonal prisons, may be related to orthorhombic distortion and abnormal spontaneous polarization direction along b axis. This study shows that tungsten bronze families are possible candidates for exploring negative thermal expansion materials.

Introduction

Controlling the thermal expansion behavior of functional materials remains a major subject in materials science.[1,2] Applications such as spacecraft,[3,4] telescope,[3,4] and Bragg grating wavelength filters[2] demand materials with nearly zero thermal expansion coefficients (TECs). Invar alloys, composed of iron (35%Fe) and nickel (65%Ni), exhibit almost zero expansion in a large range of temperatures and have been widely used in high-precision instruments.[2,5] In the last two decades, negative thermal expansion (NTE) materials are of particular interest for their rich content and abundant applications in tailoring TECs.[6-13] Understanding the thermal expansion mechanism is fundamentally important to explore NTE materials and tailor the thermal expansion responses. Tetragonal tungsten bronze (TTB, with general formula $(A2)_4(A1)_2(B1)_2(B2)_8O_{30}$ are one type of typical ferroelectric materials,[14-17] which have potential applications in dielectric, piezoelectric, ferroelectric, and optical devices. But up to now, thermal expansion properties of TTB materials are not well studied.[18-20]

Among the TTB oxides, lead potassium niobate $Pb_2KNb_5O_{15}$ (PKN) is one of the best-known compounds,[21-30] which was firstly synthesized by E. C. Subbarao as a solid solution of $PbNb_2O_6$ in 1960.[21] The piezoelectric, ferroelectric-ferroelasic coupling, optical properties, and surface-acoustic-wave (SAW) characteristics are studied previously.[21-30]

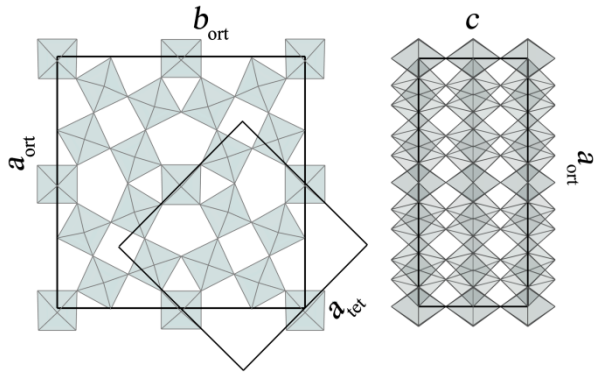

Fig. 1 Crystal structure of tetragonal tungsten bronze in a-b plane (left) and a-c plane (right).

PKN has a high Curie Temperature with $T_C \approx 460$ °C.[22,31] Above T_C, the unit cell of PKN is tetragonal with space group $P4/mbm$ (No.127) and $a_{tet} = b_{tet} \approx 12$ Å, $c \approx 4$ Å (see Figure 1). Below T_C, PKN is orthorhombic with space group $Cm2m$ (No.38) and $a_{ort} \approx b_{ort} \approx \sqrt{2}a_{tet} \approx 17$ Å, $c \approx 4$ Å[22,28] (see Figure 1), where subscript ort and tet means in orthorhombic and tetragonal coordinates respectively.

It is important to mention that in ferroelectric phase the spontaneous polarization is along b_{ort} direction, which can only be found in several lead niobate related structures in TTB, such as $Pb_2NaNb_5O_{15}$,[16] $Pb_{1-x}Ba_xNb_2O_6$ ($x < 0.3$),[32] $Pb_{2(1-}$

$_x)K_{1+x}Gd_xNb_5O_{15}$ ($x < 0.2$)[33], and $PbNb_2O_6$[14,21]. In contrast, for other lead-free or lead-less TTB-type compounds, no matter in a tetragonal or orthorhombic form, the polarization is along *c* axis (see Figure 1), such as $Sr_xBa_{1-x}Nb_2O_6$ (*P4bm*),[34] $Ba_4Na_2Nb_{10}O_{30}$ (*Cmm2*),[35] and $PbK_2LiNb_5O_{15}$ (*Pba2*).[36] In addition to the high Curie temperature and unique polar character, the lattice constant *b* (parallel to polarization direction) shrinks rapidly with the increase of temperature, which is also observed by previous researchers.[23,31] In $Sr_{0.75}Ba_{0.25}Nb_2O_6$ (SBN) [19,37], the slight NTE along *c* axis is attributed to the deviation of Nb from the center of NbO_6 octahedrons along *c* axis and the thermal motion of Nb perpendicular to the O-Nb-O linkages.[19,37] However, in polar PKN, the abnormal behavior along *b* axis in tungsten bronze is still unclear.

The purpose of this paper is to investigate the crystal structure and thermal expansion of PKN by neutron powder diffraction (NPD), high temperature XRD, nonlinear optical properties (NLO) and first-principles calculations. We discussed the role of Pb^{2+} plays on the thermal expansion and polarization mechanism in PKN. Furthermore, we demonstrated that the Pb-O covalency, especially in the large and asymmetric pentagonal sites, may be responsible for the abnormal polarization behavior and NTE along polar *b* axis.

Experimental

PKN ceramics was synthesized by solid state method. The stoichiometric raw materials, PbO, K_2CO_3 and Nb_2O_5, were ball milled in ethanol for 10 h. After drying, the fine powders were calcined in 800 °C for 4h. The calcined products were ball milled again for 10h. Then, some of the powders were made into pellets and sintered at 1150 °C covered with some calcined powder to compensate the evaporation of PbO and K_2CO_3. Some of sintered pellets were pulverized into powder for X-ray diffraction; High temperature XRD (TTRIII, Rigaku, Japan, Cu *K*α, λ = 1.5406 Å) data were collected from RT to 600 °C with a scanning rate of 4 ° / min for 2θ; The heating rate was 10 °C / min and the sample was hold for 15 min at a specified temperature to reach heat equilibrium. NPD data were collected on the BT-1 diffractometer at the center for Neutron Research at the National Institute of Standards and Technology (NIST) with a Cu monochromator (λ = 1.5403 Å) at RT and 550 °C. The macroscopical thermal expansions of ceramics were determined from dilatometric measurements using a thermo-mechanical analyzer (TMA; WCP-1) with a 2 mm sample at a heating speed of 5 °C / min. The SHG signal was detected by a FSP900 spectrometer (Edinburgh Instrument) using a nanosecond pulsed (10 Hz) 1064 nm Nd:YAG laser as the pump source. For dielectric and ferroelectric measurement, silver paste was painted as electrode onto both sides of polished pellets and fired at 550 °C for half an hour. Dielectric parameters of unpoled samples were measured as a function of frequency and temperature with an impedance analyzer (HP4192A; Hewlett-Packard, Palo Alto, CA) in the frequency range of 10^4–10^6 Hz. A triangular waveform with a frequency of 1 Hz was used to investigate room-temperature polarization curves (aixACCT, TF Analyzer 1000; Aachen, Germany).

Results and Discussion

Structure

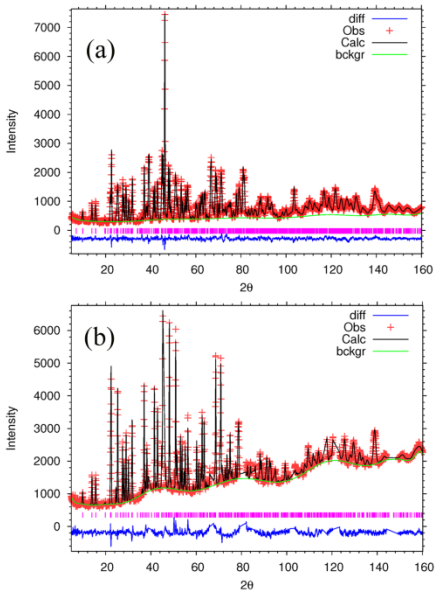

Fig. 2 Rietveld fitting patterns of NPD data at RT (a) and 550 °C (b). Observed (pluses), calculated (black line), background (green line), and difference (bottom of figure) are shown. Bars represent the Bragg positions. R_p = 4.17 %, R_{wp} = 5.52 %, R_{exp} = 3.59 %, χ^2 = 2.36 at RT and R_p = 3.19 %, R_{wp} = 4.11 %, R_{exp} = 2.37 %, χ^2 = 2.99 at 550 °C. For 550 °C, peaks from Pt substrate were excluded and not shown.

The crystal structure of PKN was firstly solved by Sciau et al. in 1999.[28] In the present work, neutron powder diffraction (NPD) was performed, which can determine the light oxygen atoms more accurately than X-Ray. Sciau's result was used as initial model with space group *Cm2m* at RT and *P4/mbm* at 550 °C. The NPD datas were analyzed with Rietveld method on a platform of software GSAS.

There are splits of Pb^{2+} in two different kinds of pentagonal sites, $Pb_p(2)$ and $Pb_p(3)$. And two identical Pb^{2+} (50% probability) distribute symmetrically in one pentagonal space, as shown in Figure S1a.

In tungsten bronze compounds, different A sites prefer different cations, depends mainly on the ionic radius.[38,39] Larger cations tend to occupy pentagonal sites, and the smaller occupy quadrangular sites. In initial refining process, the occupancy of K^+ in quadrangular sites (4e) was converged to be negative and was then fixed to be zero. Finally, K^+ were set to occupy the pentagonal sites, Pb^{2+} occupy both quadrangular sites and the rest of pentagonal sites. Then, the refined structure with space group *Cm2m* is reasonable (see Figure 2a and Table S1).

The structure with NPD data at 550 °C was refined with space group *P4/mbm* (phase transition from orthorhombic to tetragonal at about 460 °C). Since the sample was heated to a relative low temperature, sites occupancies were set to be the same as at RT. The results are shown in Figure 2b and Table S2. The crystal structures of PKN at RT and 550 °C were shown in Figure 3.

From Figure 3, we can see all cations have displacement components along $[010]_{ort}$ direction at RT. In paraelectric phase, all Nb or Pb/K atoms are in the near center of NbO_6 octahedrons or quadrangular/pentagonal sites. In ferroelectric phase, all Nb and Pb/K atoms show obvious displacements. The directions of intra-octahedron distortion of Nb are shown in arrows in Figure 3. It was found that all displacements of Nb tend to be away from the oxide ligands that bridging to Pb^{2+}. In

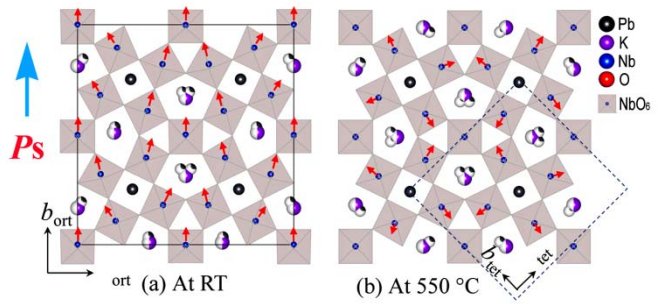

Fig. 3 Structure of PKN at RT (a) and 550 °C (b). Percent of color on atoms represent the proportion of occupancy. Unit cell of both phases are outlined. Red arrows indicate the direction Nb atoms displace in NbO_6 octahedron.

PKN, there's no polarization component along *c* axis and the net polarization component along *a* axis is zero, giving rise to total polarization along *b* axis. In displacive ferroelectrics, the spontaneous polarization P_S could be estimated by considering a purely ionic crystal and neglecting the electronic polarization: $P_S = Z\sum_i \frac{\delta z_i q_i}{V}$, where δz_i is the shift along the ferroelectric axis of the *i*th ion carrying a charge q_i, *V* is the unit cell volume and $Z = 4$. The calculated P_S of PKN is 34.9 μC/cm^2, which is similar to the value reported for $Ba_2KNb_5O_{15}$ (P_S = 32 μC/cm^2),[40] but much larger than $Sr_2KNb_5O_{15}$ (P_S = 17 μC/cm^2).[41]

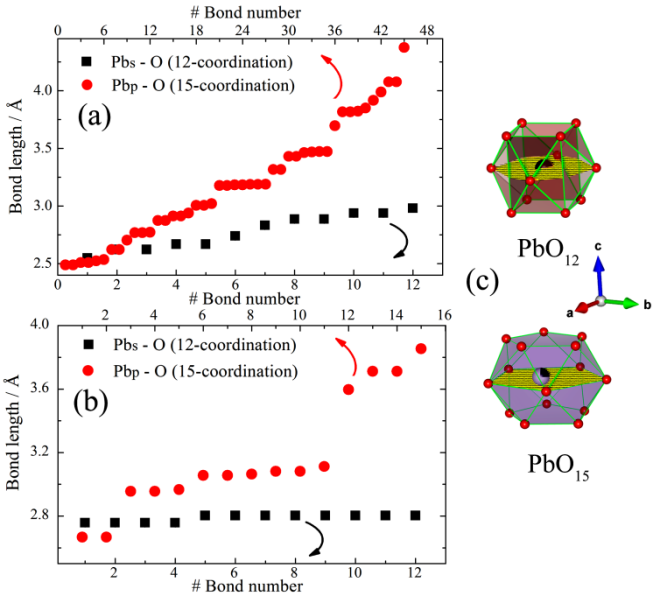

Fig. 4 Distribution of Pb-O distances in PbO_{15} and PbO_{12} polyhedrons obtained from structure refinement at RT (a) and 550 °C (b). Each point represents a kind of bond length. Errors are included, they are too small and cannot be distinguished. There are three kinds of PbO_{15} polyhedrons and 15 × 3 = 45 different Pb-O bond lengths at RT; There is only one kind of PbO_{15} polyhedron and 15 different Pb-O bond lengths at 550 °C. The structures of PbO_{15} and PbO_{12} polyhedrons at 550 °C are shown in (c).

To PKN in paraelectric phase, we can see very different oxide ligand environments on quadrangular and pentagonal sites (see Figure 4). In the equatorial plane of PbO_{15} polyhedron, the shortest Pb-O length is 2.967 Å, while the longest (Pb_p-O3(4)) is 3.8543 Å (Figure 4c and Table S4). In contrast, the Pb-O lengths in PbO_{12} polyhedron do not vary a lot (2.757 Å ≤ *d* ≤ 2.8031 Å, see Figure 4). The volume of PbO_{15} and PbO_{12} polyhedrons are 81.02 Å^3 and 51.23 Å^3 respectively, implying much more flexible space for Pb^{2+} in PbO_{15} polyhedrons to move to accommodate better coordinate environments. The strong asymmetry and large capacity in PbO_{15} polyhedrons allows Pb^{2+} to deviate from its center in *a-b* plane flexibly and strengthen the covalent bonds with O nearby.

Herein, we are interested in the effect of Pb^{2+} ions on the structural chemistry of PKN. The previous studies indicated that the lone pair electrons play a specific role in both physical and chemical properties of materials with cations Sn^{2+}, Se^{4+}, Pb^{2+}, Bi^{3+}, and so on.[42,43]

It is well known that all TTB compounds have the same crystal structure in paraelectric phase (*P4/mbm*). From paraelectric to ferroelectric phase, compared to other lead-free TTB-type compounds, the symmetry of PKN changes in *a-b* plane, not in *a-c* or *b-c* plane, and all *z*-coordinates maintain at *z* = 0 or *z* = 0.5. Compared to PKN, both $Ba_2KNb_5O_{15}$ and $Sr_2KNb_5O_{15}$[44,45] crystalize in tetragonal phase (*P4bm*) with polar direction along *c* axis. Considering the similar ionic radius of Pb^{2+} and Sr^{2+} ($r_{Sr^{2+}}$=1.44 Å, $r_{Pb^{2+}}$= 1.49 Å, CN = 12), a reasonable interpretation is to attribute to the hybridization character of Pb^{2+} with lone pair electrons: cooling the temperature down below T_C, the flexibility and asymmetry environments of Pb^{2+} along with its hybridization character drives atomic displacement along *b* direction. Similar results can be seen in $Pb_{1-x}Ba_xNb_2O_6$: with the increase of Ba content, the structure changes from orthorhombic (*Cm2m*) to tetragonal (*P4bm*).[32]

In ferroelectric perovskites ABO_3, the hybridization between B cation and O is essential to weaken the short-range electrostatic repulsions and allow the ferroelectric transitions.[6] The A-cation can affect the B-O interactions by A-O hybridization. This mechanism can be introduced to the case of PKN. Electron densities of PKN were obtained by DFT calculation, see Figure 5 and Figure S2. It can be clearly seen that the electron densities distributions around Pb, Nb, and O are quite anisotropic, while around K is almost isotropic. The electron densities on the Pb-O bonds are much larger than that on K-O bonds. The calculated results agree with the covalent character of Pb-O bonds.

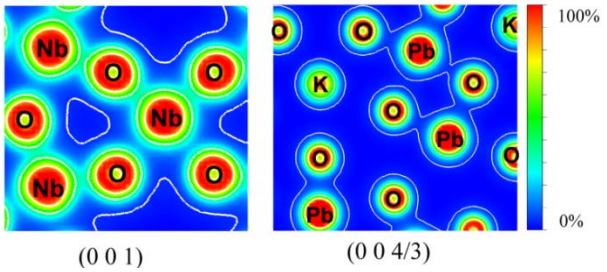

Fig. 5 Electron density difference of PKN calculated by DFT in (001) and (0 0 4/3) plane. For more details, see Supporting Information.

Thermal expansion

The HT X-Ray diffraction from RT to 600 °C was performed to determine the evolution of cell parameters, See Figure 6a-b and Figure S3. The phase transition from orthorhombic to tetragonal happens around 460 °C, which was also proved by dielectric and DSC measurements (Figure 8a and Figure S4). Figure 6a-b show that below T_C, lattice constants *a* and *c* increase upon heating, while *b* decreases with temperature. The thermal expansion coefficient (TEC) along *b* axis α_b is

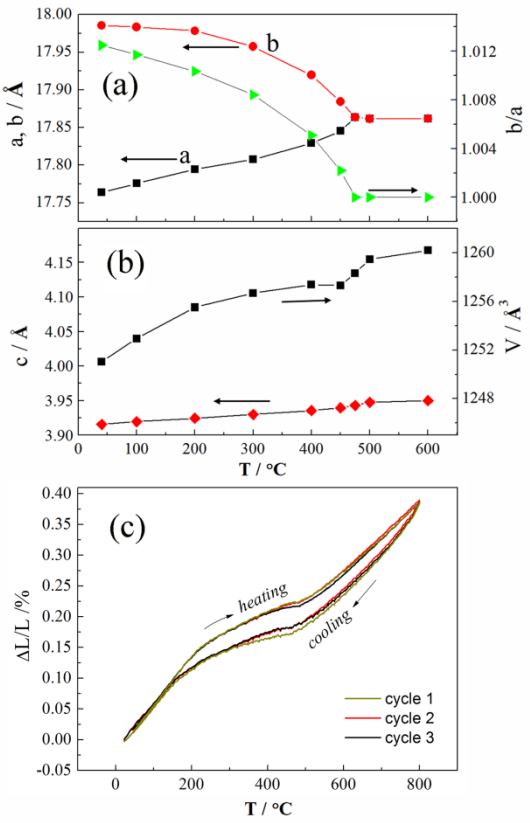

Fig. 6 (a) – (b) Lattice constants evolution of PKN at elevated temperatures; Errors are too small to be distinguished. (c) Thermal expansion measured by TMA.

1.56×10^{-5} °C^{-1}, α_a and α_c are 1.29×10^{-5} °C^{-1} and 1.62×10^{-5} °C^{-1} respectively (RT – 475 °C). The ceramic bar thermal expansion was measured by TMA, and good reproducibility on heating and cooling reveals the well thermal stability and mechanical behavior (see Figure 6c). The linear TEC α_l was 0.44×10^{-5} °C^{-1} and the average bulk TEC is $\alpha_V \approx 3\alpha_l = 1.32\times10^{-5}$ °C^{-1} in the range of 30 – 460 °C^{-1}, which is consistent with XRD measurements ($\alpha_V = 1.35\times10^{-5}$ °C^{-1}). We compared the TECs of PKN single crystals measured by other groups[31,23] and found our present results are more reliable (see Table 1).

In $PbTiO_3$-based compounds, NTE along *c* axis are strongly coupled with spontaneous polarizations and Pb/Bi-O hybridizations.[47,48] The strong Pb/Bi-O and Ti-O covalent bonds elongate TiO_6 octahedrons along polarization direction and induce large tetragonality (c/*a* = 1.06 for $PbTiO_3$).[46-50] With temperature increasing up to T_C, spontaneous polarization displacements reduce gradually to zero, and the elongated TiO_6 octahedrons shrink along *c* axis. Thus, NTE occurs. TTB structures are considered as perovskites analogue. The spontaneous polarization displacements are induced by Pb/K-O and Nb-O interations. Because of the structural flexibility and complexity in TTB oxides, the mechanism for NTE along *b* axis in PKN is more interesting. Pb-O covalency in flexible PbO_{15} polyhedrons below T_C not only distorts NbO_6 octahedrons along *b* axis, but also causes NbO_6 octahedrons cooperative rotation. Both the distortion and cooperative rotation result in the elongation along *b* axis and compression along *a* axis of the unit cell. With temperature increases, strong thermal vibration weakens both Pb-O and Nb-O bonding. All cations move towards their equilibrium positions. The

Table 1 Thermal expansion coefficients (TECs) of PKN along different axis from RT to Curie temperature reported by different authors

	TEC (10^{-5} °C^{-1})			
	a axis	*b* axis	c axis	*V*
Yamada[23,*]	1.50	-2.18	1.75	1.07
Kimura[31,*]	-0.80	-1.40	1.20	-1.00
This study	1.29	-1.56	1.62	1.35

* Data are evaluated from figures.

distortion of NbO_6 octahedrons reduces (by shrinking along *b* axis and elongating along *a* axis). At the same time, NbO_6 octahedrons rotate cooperatively, which also contributes to the NTE along *b* axis, shown in Figure 7.

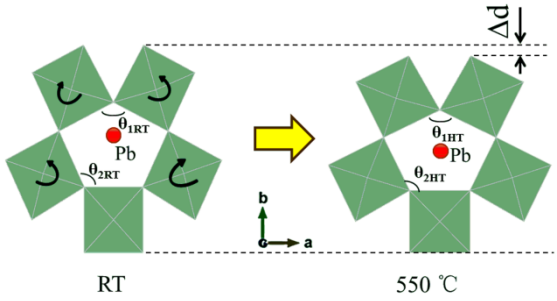

Fig. 7 Schematic presentation of NbO_6 octahedrons cooperative rotation from RT (left) to 550 °C (right) surrounding $Pb_p(2)$-O_{15} octahedron. Δ*d* indicates the compression along b axis. θ_{1RT} = 126.73 °, θ_{1HT}=128.69 °; θ_{2RT} = 114.61 °, θ_{2HT}=116.99 °. The split of Pb^{2+} are not included.

In orthorhombic phase of PKN, the distortion from tetragonal phase can be evaluated using the axis ratio *b*/*a*. At RT, *b*/*a* is 1.0125(1) and decreases gradually to 1 with temperature increases to T_C. Negative thermal expansion (NTE) is observed along *b* axis accompanied by increasing the degree of symmetry. Since ferroelectricity is closely related to structural asymmetry, the reducing of ferroelectricity as well as P_S is confirmed by the decreasing of nonlinear optical (NLO) responses measured by SHG (see Figure 8b).

Temperature dependence of dielectric properties and *P-E* hysteresis loops of PKN ceramics were also obtained (Figure 8a,c). Figure 8a shows a sharp dielectric peak at about 460 °C, indicating the ferroelectric-paraelectric transition. The maximum dielectric constants ε_{max} decrease with the increase of frequencies, but T_{max} do not show obvious change, where T_{max} is the temperature corresponding to ε_{max}. Inset shows the fitting to the modified Curie-Weiss raw. The fitted γ is 1.57, implying some extent of diffuseness during the phase transaction process. This agrees with the SHG measurement: even though the temperature is as high as 500 °C, there are still some SHG responses (Figure 8b inset). Figure 8c shows the measured *P-E* curves at different temperatures. We can see both remnant polarization (P_r) and coercive field (E_c) increase anomaly while heating. This phenomenon is attributed to the rigid of dipoles. The dipoles can not be fully switched under test conditions and become easier to switch at higher temperatures.

As discussed above, NTE along *b* axis in PKN are associated with Pb-O covalency and cooperative rotation of NbO_6 octahedrons. It's interesting to note that there is no tilt of NbO_6 octahedron since all ions do not displace along *c* axis, but along *b* axis. The attraction caused by Pb-O covalency tend to rotate NbO_6 octahedrons in *a*-*b* plane and enhances orthorhombic distortion (*b*/*a*); while the electrostatic repulsion caused by ionic K-O bonds in A sites prefer tilting it and stabilize the

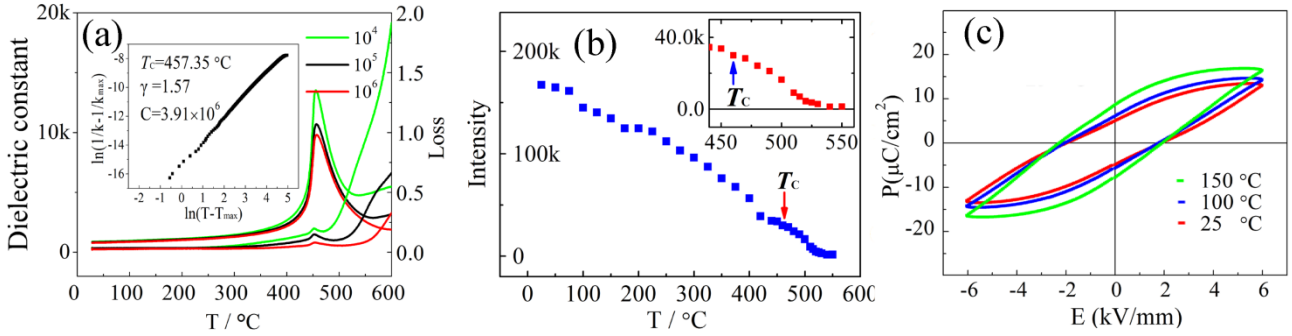

Fig. 8 (a) Temperature dependence of relative dielectric permittivity and dielectric loss; The inset shows variation of $\log(1/\varepsilon-1/\varepsilon_{max})$ with $\log(T-T_{max})$ at 10^6 Hz for PKN ceramics. T_{max} is the temperature corresponding to the dielectric constant maximum, ε_{max}; the fitted γ is 1.57, implying some extent of diffuseness. (b)Temperature dependence of second harmonic generation (SHG) response of PKN measured from RT to 550 °C. The region near T_C is shown in the inset. (c) *P-E* hysteresis loops of PKN measure from RT – 150 °C at 1Hz.

tetragonal crystal structure, such as that in $Sr_2KNb_5O_{15}$ and $Ba_2KNb_5O_{15}$.[44,45] This indicates that we can adjust the thermal expansion by modifying the ratio of ions of the two kinds or by modifying their ionic radius. For example, increasing the ratio of Pb^{2+} (or other lone pair cations), or replacing K^+ with a smaller one may enhance orthorhombic distortion and change average bulk thermal expansion coefficient from positive to negative.

Conclusions

The structure and thermal expansion properties of PKN were investigated. The transition from orthorhombic ferroelectric phase to tetragonal paraelectric phase was confirmed by XRD, NPD, and dielectric measurements. From RT to ferroelectric Curie temperature (460 °C), PKN shows a negative thermal expansion behavior along *b* axis, and the anisotropic thermal expansion coefficients are $\alpha_a = 1.29\times10^{-5}$ °C^{-1}, $\alpha_b = -1.560\times10^{-5}$ °C^{-1}, and $\alpha_c = 1.62\times10^{-5}$ °C^{-1}, respectively. SHG confirms the increase of symmetry and decrease of spontaneous polarization with the increase of temperature. NTE along *b* axis is accounted by distortion and cooperative rotation of NbO_6 octahedrons, which is also related to the Pb-O covalency. It is believed that Pb-O covalency, especially in the pentagonal sites, is the reason for the spontaneous along *b* axis. The mechanism may be used to control TECs and explore negative thermal expansion materials with tungsten bronze structures.

Acknowledgements

This work was supported by National Natural Science Foundation of China (Grant Nos. 91022016, 21031005, 21231001), Program for Changjiang Scholars and Innovative Research Team in University (IRT1207). The calculations were performed on the Quantum Materials Simulator of USTB.

Notes and References

[a] Department of Physical Chemistry, University of Science and Technology Beijing, Beijing 100083, China; Tel: +86-10-62334200; Fax: +86-10-62332525; E-mail: xing@ustb.edu.cn.
[b] NIST Center for Neutron Research, National Institute of Standards and Technology, Gaithersburg, Maryland 20899-6102, United States
[c] Department of Materials Science and Engineering, University of Maryland, College Park, MD 20742-2115, United States
[d] Department of Chemistry, University of Science and Technology Beijing, Beijing 100083, China
[e] Key Laboratory of New Processing Technology for Nonferrous Metals and Materials, Ministry of Education, Guilin University of Technology, Guilin 541004, China

† Electronic Supplementary Information (ESI) available: [High temperature XRD patterns; C_p curves measured by DSC; the details for DFT calculation; atomic positions at RT and 550 °C; Pb-O bond lengths in PbO_{15} and PbO_{12} polyhedrons, and CIF files]. See DOI: 10.1039/b000000x/

1. A. L. Goodwin, *Nature Nanotech.*, 2008, **3**, 710-711.
2. P. Mohn, *Nature*, 1999, **400**, 18-19.
3. H. Akitaya, M. Iye, K. Okita and e. a. Sato, In Application of zero-expansion pore-free ceramics to a mirror of an astronomical telescope, 2008, pp 70183H-70183H-12.
4. Strock, J. D. In Development of Zero Coefficient of Thermal Expansion composite tubes for stable space structures, 1992, pp 223-230.
5. C. E. C. R. Guillaume, *Acad. Sci.*, 1897, **125**, 4.
6. T. A. Mary, J. S. O. Evans, T. Vogt and A. W. Sleight, *Science*, 1996, **272**, 90-92.
7. A. P. Ramirez, G. Ernst, C. Broholm and G. R. Kowach, *Nature*, 1998, **396**, 147-149.
8. I. Bull, P. Lightfoot, L. A. Villaescusa, L. M. Bull, R. K. B. Gover, J. S. O. Evans, R. E. Morris, *J. Am. Chem. Soc.*, 2003, **125**, 4342.
9. A. L. Goodwin, M. Calleja, M. J. Conterio, M. T. Dove, J. S. O. Evans, D. A. Keen, L. Peters, M. G. Tucker, *Science*, 2008, **319**, 794-797.
10. M. Azuma, W. T. Chen, H. Seki, M. Czapski, S. Olga, K. Oka, M. Mizumaki, T. Watanuki, N. Ishimatsu, N. Kawamura, S. Ishiwata, M. G. Tucker, Y. Shimakawa and J. P. Attfield, *Nat. Commun.*, 2011, **2**, 347.
11. C. Wang, L. Chu, Q. Yao, Y. Sun, M. Wu, L. Ding, J. Yan, Y. Na, W. Tang, G. Li, Q. Huang, J. W. Lynn, *Phys. Rev. B*, 2012**, 85**, 22013.
12. N. Lock, M. Christensen, C. J. Kepert and B. B. Iversen, *Chem. Commun.*, 2013, **49**, 789-791.
13. J. Chen, L. Fan, Y. Ren, Z. Pan, J. Deng, R. Yu and X. Xing, *Phys. Rev. Lett.*, 2013, **110**.

14. M. H. Francombe and B. Lewis, *Acta Cryst.*, 1958, **11**, 696-703.
15. M. H. Francombe, *Acta Cryst.*, 1960, **13**, 131-140.
16. J. Ravez and B. Elouadi, *Mater. Res. Bull.*, 1975, **10**, 1249-1254.
17. X. L. Zhu, X. M. Chen and G. Brennecka, *J. Am. Ceram. Soc.*, 2012, **95**, 3185-3191.
18. J. L. Mukherjee and F. F. Y. Wang, *Am. Ceram. Soc. Bull.*, 1970, **49**, 418-418.
19. S. B. Qadri, J. A. Bellotti, A. Garzarella and D. H. Wu, *Appl. Phys. Lett.*, 2005, **86**, 251914-251913.
20. N. G. Chernorukov, A. V. Knyazev, N. Y. Kuznetsova and I. V. Ladenkov, *Phys. Solid State*, 2011, **53**, 292-298.
21. E. C. Subbarao and G. Shirane, *J. Chem. Phys.*, 1960, **32**, 1846-1851.
22. T. Yamada, *Appl. Phys. Lett.*, 1973, **23**, 213-214.
23. J. Nakano and T. Yamada, *J. Appl. Phys.*, 1975, **46**, 2361-2365.
24. T. Yamada, *J. Appl. Phys.*, 1975, **46**, 2894-2898.
25. J. Ravez, B. Elouadi and P. Hagenmuller, *Ferroelectrics*, 1978, **21**, 583-585.
26. H. Yamauchi, *Appl. Phys. Lett.*, 1978, **32**, 599.
27. R. M. O'Connell, *J. Appl. Phys.*, 1978, **49**, 3324.
28. P. Sciau, G. Calvarin and J. Ravez, *Acta Crystallogr. Sect. B: Struc. Sci.*, 1999, **55**, 459-466.
29. K. Sambasiva Rao, P. Murali Krishna and D. Madhava Prasad, *Phys. Status Solidi B*, 2007, **244**, 2267-2287.
30. A. Belboukhari, Z. Abkhar, E. Choukri, Y. Gagou, N. Abdelmoula, R. Elmoznine, D. Mezzane, H. Khemakhem, M. El Marssi, A. Razumnaya, I. Raevski and I. Luk'yanchuk, *Ferroelectrics*, 2013, **444**, 116-124.
31. H. Kimura, K. Maiwa, A. Miyazaki, H. Nakamura, Z. Cheng and K. Chinna Venkadasamy, *Jpn. J. Appl. Phys.*, 2004, **43**, 6658-6661.
32. M. Venet, F. L. Zabotto, J. A. Eiras and D. Garcia, *J. Appl. Phys.*, 2009, **105**, 124106.
33. Y. Amira, Y. Gagou, A. Menny, D. Mezzane, A. Zegzouti, M. Elaatmani and M. El Marssi, *Solid State Commun.*, 2010, **150**, 419-423.
34. S. Podlozhenov, H. A. Graetsch, J. Schneider, M. Ulex, M. Woehlecke and K. Betzler, *Acta Crystallogr. B*, 2006, **62**, 960-965.
35. P. Labbe, H. Leligny, B. Raveau, J. Schneck and J. C. Toledano, *J. Phys.: Condens. Matter*, 1990, **2**, 25-43.
36. P. Saint-Grégoire, Y. Gagou and T. Badeche, *Ferroelectrics*, 2008, **376**, 17-24.
37. S. B. Qadri, J. A. Bellotti, A. Garzarella, T. Wieting, D. H. Wu and N. A. Mahadik, *Appl. Phys. Lett.*, 2006, **89**, 222911-222913.
38. M. Elaatmani, A. Zegzouti, F. Capitelli, A. G. G. Moliterni, A. Migliori and G. Calestani, *Z. Kristallogr.*, 2003, **218**, 26-31.
39. X. L. Zhu, X. Q. Liu and X. M. Chen, *J. Am. Ceram. Soc.*, 2011, **94**, 1829-1836.
40. E. A. Giess, B. A. Scott, G. Burns, D. F. O'Kane and A. Segmuller, *J. Am. Ceram. Soc.*, 1969, **52**, 276-281.
41. G. Burns and A. Smith, *IEEE J. Quantum Elect.*, 1968, **4**, 584-587.
42. A. Walsh and G. W. Watson, *J. Solid State Chem.*, 2005, **178**, 1422-1428.
43. P. S. Halasyamani, *Chem. Mat.*, 2004, **16**, 3586-3592.
44. S. Lanfredi, C. X. Cardoso and M. A. L. Nobre, *Mater. Sci. Eng. B-Adv.*, 2004, **112**, 139-143.
45. W. Zhang, N. Kumada, T. Takei, Y. Yonesaki and N. Kinomura, *Mater. Res. Bull.*, 2007, **42**, 844-850.
46. R. E. Cohen, *Nature*, 1992, **358**, 136-138.
47. J. Chen, K. Nittala, J. S. Forrester, J. L. Jones, J. Deng, R. Yu and X. Xing, *J. Am. Chem. Soc.*, 2011, **133**, 11114-11117.
48. J. Chen, X. Xing, C. Sun, P. Hu, R. Yu, X. Wang and L. Li, *J. Am. Chem. Soc.*, 2008, **130**, 1144-1145.
49. M. Yashima, K. Omoto, J. Chen, H. Kato and X. Xing, *Chem. Commun. (Cambrideg, U.K.)*, 2011, **23**, 3135-3137.
50. Y. Kuroiwa, S. Aoyagi, A. Sawada, J. Harada, E. Nishibori, M. Takata and M. Sakata, *Phys. Rev. Lett.*, 2001, **87**, 217601.

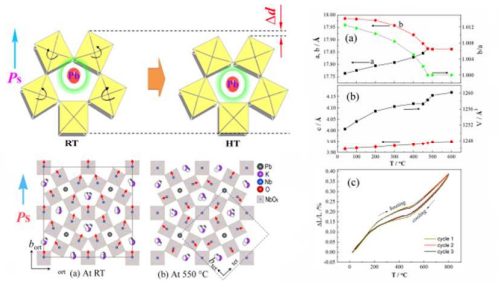

Distortion and cooperative rotation of NbO_6 octahedrons are directly responsible for negative thermal expansion coefficient along polar b axis. Pb-O covalency, especially in the large and asymmetry pentagonal prisons, may be related to orthorhombic distortion, abnormal spontaneous polarization direction, and negative thermal expansion along b axis. This study shows that tungsten bronze families are possible candidates for exploring negative thermal expansion materials.